

MANGANESE OXIDE BASE ELECTRODE MATERIALS WITH POROUS STRUCTURES FOR SUPERCAPACITOR

Y. LV, G. DONG^{*}, L. LI, J. KANG, W. HAN

College of Materials Science and Engineering, North China University of Science and Technology, Hebei Provincial Key Laboratory of Inorganic Nonmetallic Materials, Tangshan Hebei, 063009, China

MnO₂-based materials with porous structures comprising nanorods or nanowires and nanoparticles were synthesized via a facilely chemical precipitation method. Diverse manganese sources and doping amounts of cobalt and chromium ions were designed to gain MnO₂-based electrode materials with remarkable electrochemical performances. Pure MnO₂ prepared by MnAc₂ exhibited a superior specific capacitance of 97.34 F g⁻¹ at the current density of 200 mA g⁻¹. MnO₂-based materials with cobalt adulteration at a Co/Mn molar ratio of 1:50 (MnO₂-Co-50-1) revealed a specific capacitance of 116.6 F g⁻¹ at the current density of 200 mA g⁻¹. While MnO₂-based materials with chromium adulteration at a Cr/Mn molar ratio of 1:20 (MnO₂-Cr-20-1) showed up a higher specific capacitance of 144.26 F g⁻¹ at the current density of 200 mA g⁻¹. It is worth mentioning that all electrochemical tests were measured with a wide voltage region of 0-1V in a neutral electrolyte of 1M Na₂SO₄ aqueous solution. Even so materials still showed up an excellent cycling stability, and MnO₂-Co-50-1 retained 101.69% of capacitance (58.02 F g⁻¹) at a scan rate of 100 mV s⁻¹ after 2500 cycles while MnO₂-Cr-20-1 retained 86% of capacitance (72.83 F g⁻¹) at a scan rate of 100 mV s⁻¹ after 2500 cycles. All these profited greatly from materials' ideally porous network structures, which offers an efficient structural platform for fast energy storage.

(Received November 8, 2017; Accepted April 5, 2018)

Keywords: Manganese oxide; Cobalt and chromium adulteration; Electrode material; Supercapacitor

1. Introduction

Basing on the extremely urgent demand of a new energy storage device combining high power density and high energy density, more and more attentions have been focused on supercapacitor, also owing to its extra excellent performances of long cycling life and environmental friendliness^[1-3]. Thus supercapacitor has been regarded as a most promising energy storage component and has a wide applications ranging from rail transit, consumer electronics to wind and solar energy storage as well as energy recycling devices^[4-6]. For further application, the innovation of electrode materials playing a vital role in supercapacitors has never been given up^[7,8].

Compared with carbon-based materials and conducting polymer materials, metal oxides attract much attention owing to their extra chemical energy storage and thermal stability^[9-13]. And among these, Ruthenium oxide was known at the earliest for its high pseudo-capacitance in a highly acidic electrolyte, which leads to a high power density^[14,15]. While the high cost and poor capacitance retention with respect to cycling time, resulting from the instability of metal oxides in acidic solution, of ruthenium oxide limit its extensive application^[16-18]. Then the capacitive performances of transition metal compounds like cobalt or nickel oxides/hydroxides and

^{*} Corresponding author: dgxlyn1218@126.com

manganese oxides were gradually studied for alternative materials^[19-22]. Of the various substitutions, manganese dioxide occupies an important position due to its particularly wide range of voltage in a neutral electrolyte system^[23-25]. Besides manganese oxide's lower cost and admirable capacitance-property also make a great contribution to its bright prospects^[26-28]. Even so the poor electron conductivity, a general weakness of metal oxides, brings about great space to promote the electrochemical performances of manganese dioxide^[29,30].

Herein this paper synthesized a series of MnO₂-based materials with porous structures by a simple and effective precipitation method and attempted to change manganese sources and make lattice imperfections by partially replacing manganese ions with cobalt and chromium ions to improve material's electrochemical performances. Among all MnO₂-based materials, MnO₂-Co-50-1 and MnO₂-Cr-20-1 displayed a superior specific capacitance of 116.6F g⁻¹ and 144.26F g⁻¹ at 200mA g⁻¹, respectively. Besides the capacitance retention of MnO₂-Co-50-1 was 101.69% while that of MnO₂-Cr-20-1 was 86% at 100mV s⁻¹ after 2500 cycles.

2. Experimental

2.1. synthesis of MnO₂-based materials

All of chemical reagents used in this experiment were of analytical grade without any further purification. MnO₂-based materials were synthesized by a facile precipitation method and experiment consists of two parts: preparation of pure MnO₂ with senior performance and synthesis of MnO₂-based materials with cobalt or chromium doping.

In order to investigate the effects of different raw materials on electrochemical performances of pure MnO₂ and modify performances based on better basis materials, two kinds of raw materials were tried in the synthesis of pure MnO₂. Firstly, 75mmol MnCl₂ and 50mmol KMnO₄ were dissolved in 150mL and 100mL deionized water respectively to gain 0.5 M MnCl₂ and 0.5 M KMnO₄ uniform solution by magnetic stirring for 15 min at room temperature. Then MnCl₂ solution was slowly added to KMnO₄ solution drop by drop with persistently magnetic stirring for 10h. Finally, a brown MnO₂ suspension was dried at 100°C for 4h in air after it was filtrated and washed completely with distilled water and alcohol. Another pure MnO₂ powders were synthesized via the same experiment procedure except replacing MnCl₂ with MnAc₂ of the same mole. MnO₂-based materials with cobalt/chromium doping were synthesized via the same experimental process except for that CoAc₂/CrAc₂ partly substituted for MnAc₂ on the basis of Co/Mn or Cr/Mn molar ratio of 1:10, 1:20, 1:50 and 1:100.

For convenience, pure MnO₂ prepared by MnCl₂ and MnAc₂ were called after MnO₂-pure-1 and MnO₂-pure-2, respectively. MnO₂-based materials with cobalt doping (MnO₂-Co-based materials) at a Co/Mn molar ratio of 1:10, 1:20, 1:50 and 1:100 were named MnO₂-Co-10-1, MnO₂-Co-20-1, MnO₂-Co-50-1 and MnO₂-Co-100-1, separately; MnO₂-based materials with chromium doping (MnO₂-Cr-based materials) at a Cr/Mn molar ratio of 1:10, 1:20, 1:50 and 1:100 were called after MnO₂-Cr-10-1, MnO₂-Cr-20-1, MnO₂-Cr-50-1 and MnO₂-Cr-100-1, respectively.

2.2 Materials' characterizations

MnO₂-based materials were characterized by X-ray diffraction (XRD) operating on a Rigaku D/MAX2500PC with Cu K α ($\lambda=1.54178 \text{ \AA}$) radiation and scanning electron microscope (SEM) carried on a SIGMA scanning electron microscope made by CARL ZIESS.

2.3 Preparation of electrodes

MnO₂-based electrodes were fabricated by a coating method. Briefly, mixed MnO₂-based materials with acetylene black and polyvinylidene fluoride (PVDF) in a mass ratio of 80:10:10 as well as proper nitrogen methyl pyrrolidone (NMP) to obtain an uniform slurry. Then the homogenized slurry was coated on nickel foam substrates with a thickness of about 5mm by a small coating machine and dried at 60°C for 6h to remove the solvent. At last, semi-finished

electrodes were pressed on a powder compressing machine under a pressure of 20MPa for 60s, which followed by punched to rounded slices with a diameter of 8mm for measurements.

2.4 Electrochemical measurements

All electrochemical measurements consisting of cyclic voltammetry (CV), chronopotentiometry (CP) and cycling tests were carried on a CHI660E electrochemical station (Chenhua corp. shanghai) by using a three-electrode system with a wide voltage window from 0V to 1V in 1M Na₂SO₄ electrolyte. The mass specific capacitance (F g⁻¹) of MnO₂-based electrode materials can be calculated from CV (C_1) and CP (C_2) curves via Eq.(1) and (2) respectively, where I_1 (A) is the respond current, I_2 (A) is the discharge current, v (V s⁻¹) is the scan rate, Δt (s) is the discharge time, m (g) is the mass of electroactive materials, ΔV (V) is the voltage window^[31,32].

$$C_1 = \frac{\int I_1 dV}{m v \Delta V} \quad (1)$$

$$C_2 = \frac{I_2 \Delta t}{m \Delta V} \quad (2)$$

3. Results and discussions

Fig. 1 shows the XRD patterns of MnO₂-based samples: pure MnO₂ powders synthesized by two-type raw materials and MnO₂-based powders with cobalt/chromium doping. As shown in Fig. 1a, two-type pure MnO₂ powders have mostly similar diffraction peaks at 12.8°, 18.1°, 28.8°, 37.5°, 41.9°, 49.8°, 60.3°, 65.1°, 68.1° and 72.7°, and these 2 θ values correspond respectively to the (110), (200), (310), (211), (301), (411), (521), (002), (202) and (312) planes of tetragonal alpha-MnO₂ (JCPDS No.44-0141). Besides extra diffraction peaks of pure MnO₂ prepared by MnCl₂ observed at 21.9°, 56.6° and 67.6° are corresponding to the crystal planes of (101) of beta-MnO₂ (JCPDS No.43-1455), (211) of beta-MnO₂ (JCPDS No.24-0735) and (710) of alpha-MnO₂ (JCPDS No.44-0141) respectively. In short, the principal crystalline phase of pure MnO₂ prepared by MnAc₂ was alpha-MnO₂, while that of pure MnO₂ gained in the presence of MnCl₂ was a combination of alpha-MnO₂ and beta-MnO₂. The variations of crystal structures resulting from partly replacing manganese ion with cobalt or chromium ions are displayed in Fig. 1b-c. Noted from Fig. 1b-c, the adulteration of cobalt or chromium ions has a great influence on the crystal phase and almost all major crystal structures of samples with ionic adulteration transform into a combination of alpha-MnO₂ and amorphous MnO₂, except that MnO₂-Co-10-1 maintains the same principal crystalline phase of alpha-MnO₂ with the initial pure MnO₂ prepared by MnAc₂.

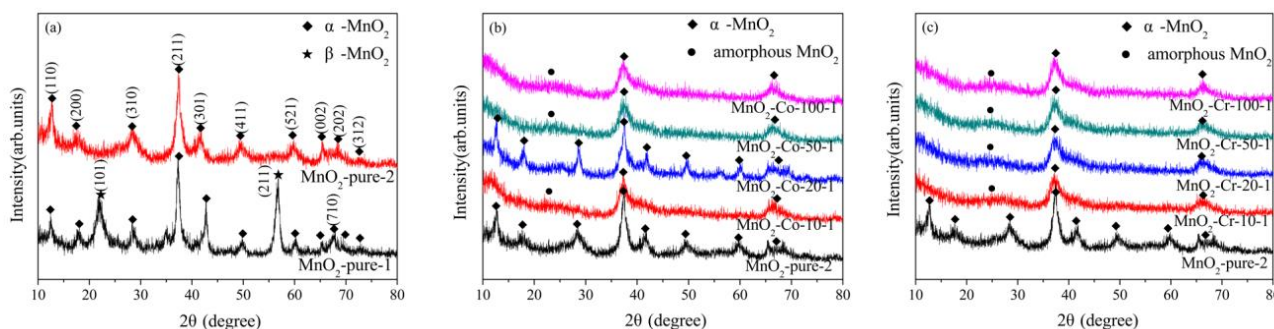


Fig. 1. XRD patterns of (a) pure MnO₂ materials, (b) MnO₂-Co-based materials and (c) MnO₂-Cr-based materials.

Fig. 2 shows the SEM images of MnO₂-based materials: Fig.2a-b corresponds with MnO₂-pure-1 and MnO₂-pure-2; Fig.2c-f corresponds to MnO₂-Co-10-1, MnO₂-Co-20-1, MnO₂-Co-50-1 and MnO₂-Co-100-1, respectively; Fig.2g-j corresponds to MnO₂-Cr-10-1, MnO₂-Cr-20-1, MnO₂-Cr-50-1 and MnO₂-Cr-100-1, respectively. As depicted in Fig.2a-b, MnO₂-pure-1 consists of nanorods with a diameter of about 40nm and nanosheets with a thickness of about 20nm, while MnO₂-pure-2 is composed of nanowires with a diameter of about 8nm and these nanowires densely interconnected with each other. It's concluded that pure MnO₂ samples prepared by different raw materials have utterly diverse morphology. The effects of cobalt-doping amounts on MnO₂-based materials' morphology were shown in Fig.2c-f. Compared with Fig.2b, it is no hard to find that a handful of cobalt doping leads to the disintegration of MnO₂ nanowires and the formation of mushroom-like nanoparticles with a diameter of about 17nm, and that nanowires with a diameter of about 1nm form a network structure with nanoparticles filled in. As observed in Fig.2c-f, with the increasing of cobalt doping, nanowires and nanoparticles transformed into nanorod with a diameter of about 40nm and particles with a state of aggregation, which brings about the decreasing of materials' effective surface areas in some degree and possibly causes an unsatisfactory performance. Besides the adulteration of chromium ion contributes to the forming of materials' porous structures consisting of thin nanowires and cotton-like nanoparticles, which can be clearly confirmed by Fig.2j. As displayed in Fig.2g-j, the loose structure developed completely with the adding of doping dosage and an optimal loose structure visually was obtained at a Cr/Mn molar ratio of 1:20, which probably provided an excellent structural foundation for admirably electrochemical performances.

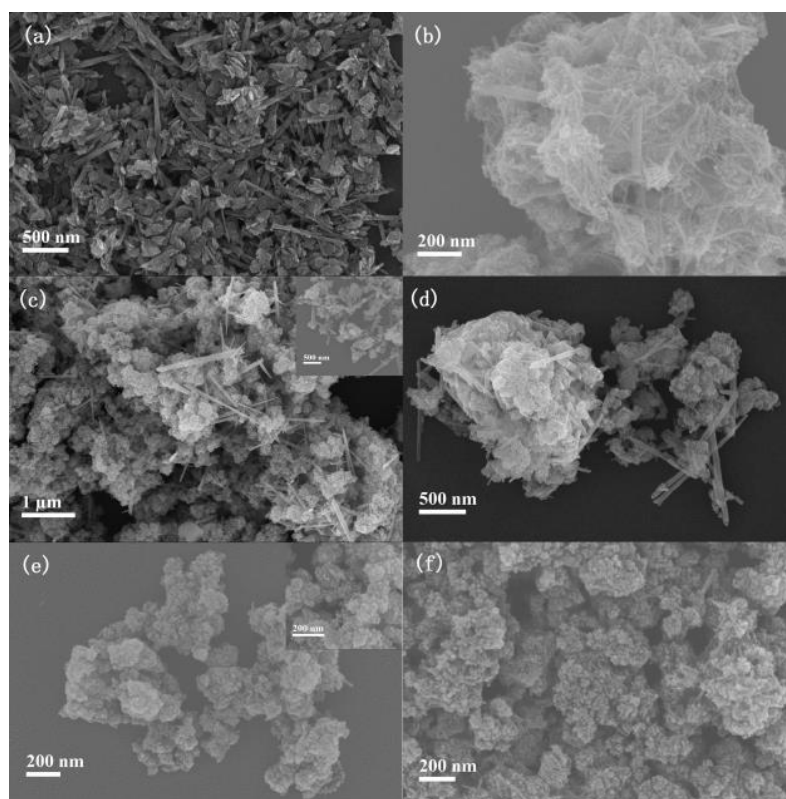


Fig. 2.1. SEM images of (a) MnO₂-pure-1, (b) MnO₂-pure-2 and (c) MnO₂-Co-10-1, (d) MnO₂-Co-20-1, (e) MnO₂-Co-50-1, (f) MnO₂-Co-100-1

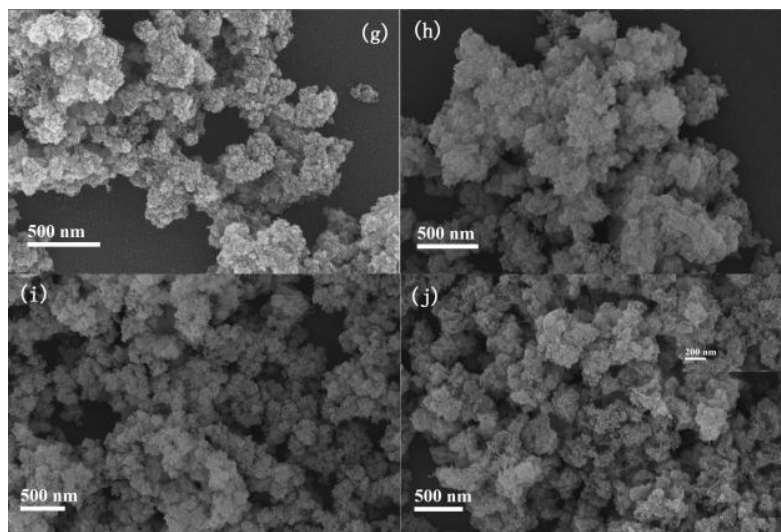


Fig. 2.2. SEM images of (g) $\text{MnO}_2\text{-Cr-10-1}$, (h) $\text{MnO}_2\text{-Cr-20-1}$, (i) $\text{MnO}_2\text{-Cr-50-1}$, (j) $\text{MnO}_2\text{-Cr-100-1}$.

The electrochemical performances of MnO_2 -based materials were measured by CV and CP tests with a wide range of voltage from 0V to 1V in 1M Na_2SO_4 aqueous solution. As seen in Fig.3a-b, MnO_2 showed an ideal capacity with the CV curves closing to a quasi-rectangular shape and $\text{MnO}_2\text{-pure-2}$ exerted a specific capacitance of 97.34F g^{-1} at 200mA g^{-1} , more than twice of the specific capacitance of $\text{MnO}_2\text{-pure-1}$ at the same level. Thus the discrepancy of manganese sources led to different crystal structures and morphology, and then resulted in distinctly electrochemical performances of pure MnO_2 materials.

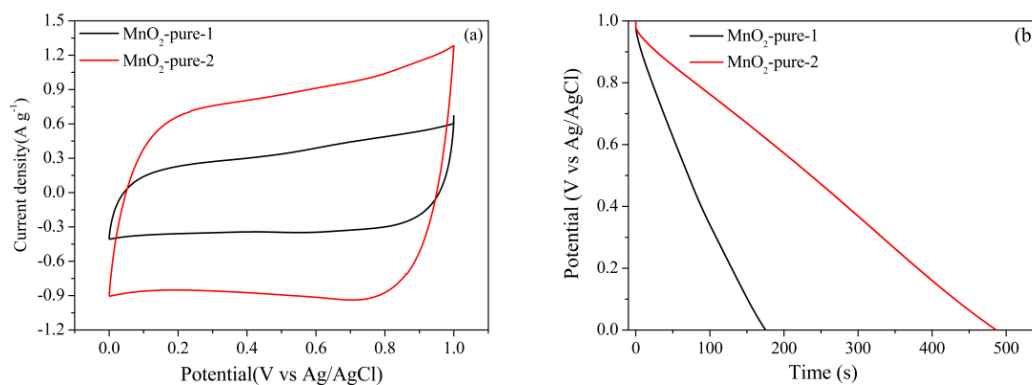


Fig. 3. (a) CV curves of pure MnO_2 materials at a scan rate of 10mV s^{-1} . (b) CP curves of pure MnO_2 materials at a current density of 200mA g^{-1} .

Contrasted with $\text{MnO}_2\text{-pure-2}$, the properties of MnO_2 -based materials with different doping amounts of cobalt and chromium ions were shown in Fig.4a-d. Moderate adulteration of cobalt ion can effectively improve the capacitive behaviors of MnO_2 -based materials and $\text{MnO}_2\text{-Co-50-1}$ showed up the highest specific capacitance of 116.6F g^{-1} at 200mA g^{-1} among all cobalt-doping MnO_2 materials, which can be confirmed in Fig.4a-b. On the contrary in Fig.4c-d, all MnO_2 -based materials with chromium superseding possessed universally excellent

electrochemical performances than MnO_2 -pure-2, and among these MnO_2 -Cr-20-1 exhibited a highest specific capacitance of 144.26F g^{-1} at 200mA g^{-1} .

The influences of current density and cycle numbers on the capacitive behaviors of MnO_2 -Co-50-1 and MnO_2 -Cr-20-1 were investigated in Fig.5a-d. From Fig.5a-b, it is obviously observed that the specific capacitance of samples reduced with the increasing of current density, resulting from that only the outer surface of materials can be utilized in the storage of energy at a high current density. Thus MnO_2 -Co-50-1 and MnO_2 -Cr-20-1 retained about 52.31% (61F g^{-1}) and 63.64% (91.8F g^{-1}) of the initial specific capacitance respectively when the current density enhanced from 200mA/g to 2A g^{-1} . Besides cycling life tests over 2500 cycles for MnO_2 -Co-50-1 and MnO_2 -Cr-20-1 were also evaluated by CV at 100mV s^{-1} and the results were shown in Fig.5c-d. As further proven by the stable CV curves, MnO_2 -Co-50-1 exhibited an excellent cycling stability with a capacitance retention of 101.69% after 2500 cycles, possessing a specific capacitance of 58.02F g^{-1} in the first cycle and a higher specific capacitance of 59F g^{-1} in the 2500th cycle, in virtue of the activation of the electrode materials. At the same time, MnO_2 -Cr-20-1 showed a specific capacitance of 72.83F g^{-1} initially and retained 86% (14% lose) of capacity (62.67F g^{-1}) after 2500 cycles. And yet for all that, MnO_2 -Cr-20-1 revealed a much higher capacitance than MnO_2 -Co-50-1 throughout. In general, the superior performances of MnO_2 -Co-50-1 and MnO_2 -Cr-20-1 greatly profit from their imperfect crystal structure and porous morphology.

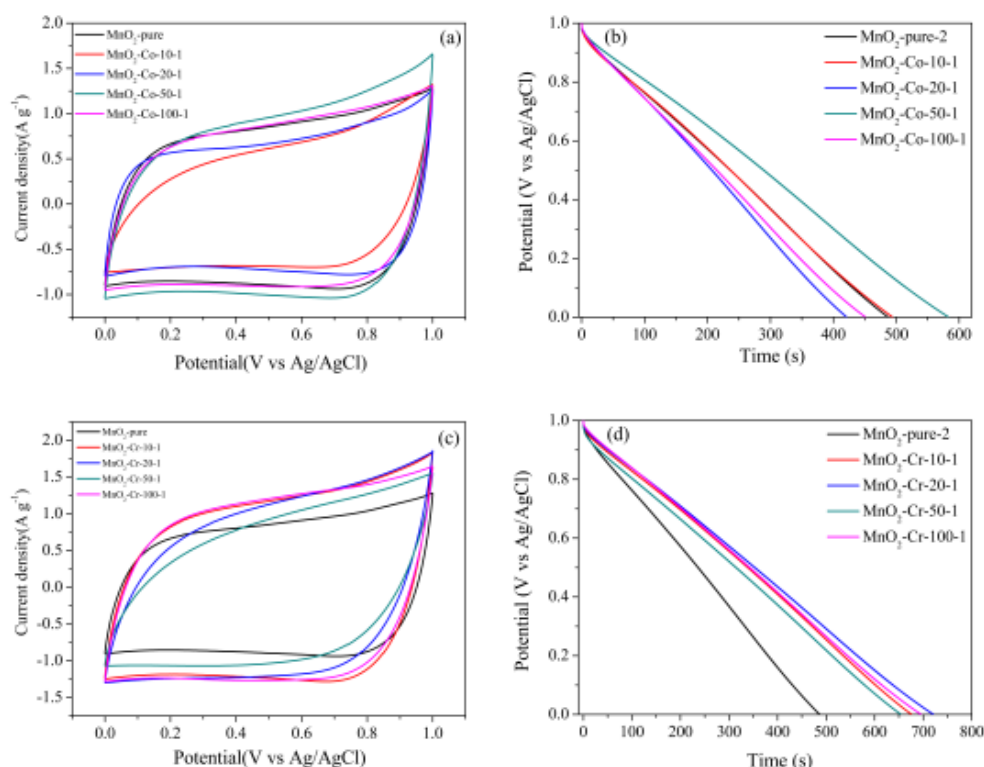


Fig. 4. CV curves of (a) MnO_2 -Co-based materials and (c) MnO_2 -Cr-based materials at 10mV s^{-1} . CP curves of (b) MnO_2 -Co-based materials and (d) MnO_2 -Cr-based materials at 200mA g^{-1} .

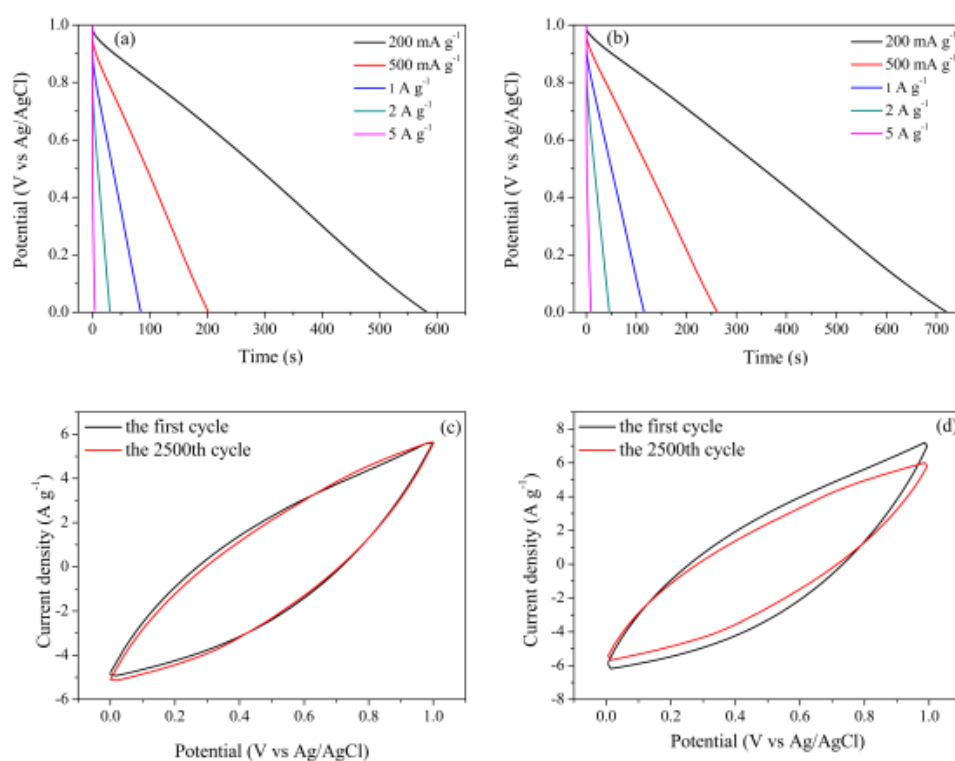


Fig. 5. CP curves of (a) MnO₂-Co-50-1 and (b) MnO₂-Cr-20-1 at various current densities. cycling performances of (c) MnO₂-Co-50-1 and (d) MnO₂-Cr-20-1.

4 Conclusions

In summary, MnO₂-based materials with different raw materials and various doping amounts of cobalt and chromium ions were prepared via a simple method of precipitation. MnO₂-pure-2 synthesized by MnAc₂ possessed a larger specific surface with nanowires staggered on each other and exhibited a higher specific capacitance (97.34 F g⁻¹ at 200 mA g⁻¹) than MnO₂-pure-1 gained by MnCl₂. To further improve materials' properties on this basis, manganese ions were partly replaced by cobalt and chromium ions with diverse Co/Mn or Cr/Mn molar rates and the adulteration of heterogeneous ions effectively created a more porous network structure with fine nanowires and nanoparticles, which provides an efficient structural foundation for electrochemical performances of materials. And what is notable is that all electrochemical measurements were carried on with a wide voltage range from 0V to 1V in a neutral electrolyte. Even so MnO₂-Co-50-1 and MnO₂-Cr-20-1 revealed an optimal capacitance behavior among all samples with the same ion-doping type. Specifically speaking, MnO₂-Co-50-1 showed up a specific capacitance of 116.6 F g⁻¹ at the current density of 200 mA g⁻¹ and retained 101.69% of capacitance at the scan rate of 100 mV s⁻¹ after 2500 cycles. While MnO₂-Cr-20-1 displayed a higher specific capacitance of 144.26 F g⁻¹ at the current density of 200 mA g⁻¹ and retained 86% of capacitance at the scan rate of 100 mV s⁻¹ after 2500 cycles.

Acknowledgements

This work was supported by National International Technology Cooperation Plan (Grant No.2014DFR50570).

References

- [1] L. Bao, J. Zang, X. Li, *Nano Lett.* **11** (3), 1215 (2011).
- [2] A. Bello, O. O. Fashedemi, F. Barzgar, M. J. Madito, D. Y. Momodu, T. M. Masikhwa, J. K. Dangbegnon and N. Manyala, *J. Alloys Compd.* **681**, 293 (2016).
- [3] Y. Chang, Y. W. Sui, J. Q. Qi, L. Y. Jiang, Y. Z. He, F. X. Wei and Q. K. Meng, *Mater. Lett.* **176**, 274 (2016).
- [4] A. Gambou-Bosca and D. Belanger, *J. Electrochem. Soc.* **162** (5), A5115 (2015).
- [5] Y. Gao, S. Chen, D. Cao, G. Wang and J. Yin, *J. Power Sources*, **195** (6), 1757 (2010).
- [6] X. L. Guo, X. Y. Liu, X. D. Hao, S. J. Zhu, F. Dong, Z. Q. Wen and Y. X. Zhang, *Electrochim. Acta*, **194**, 179 (2016).
- [7] J. Hu, F. Qian, G. Song and L. Wang, *Nanoscale Res. Lett.* **11** (1), 257 (2016).
- [8] J. Yang, H. Wang and R. F. Wang, *J. Mater. Sci.-Mater. Electron.* **28** (9), 6481 (2017).
- [9] G. P. Wang, L. Zhang and J. J. Zhang, *Chem. Soc. Rev.* **41** (2), 797 (2012).
- [10] X.Q. Li, S.Y. Lin, M.Y. Zhang, G. Jiang, H. Gao, *Nano*, **11** (5), 1650050 (2016).
- [11] M.Y. Ho, P.S. Khiew, D. Isa, T.K. Tan, W.S. Chiu, C.H. Chia, *Nano*, **9** (06), 1430002 (2014).
- [12] J. Huang, J. Zhu, K. Cheng, Y. Xu, D. Cao and G. Wang, *Electrochim. Acta*, **75**, 273 (2012).
- [13] J. Liu, J. Jiang, C. Cheng, H. Li, J. Zhang, H. Gong and H. J. Fan, *Adv. Mater.* **23** (18), 2076 (2011).
- [14] Z. S. Wu, D. W. Wang, W. Ren, J. Zhao, G. Zhou, F. Li and H. M. Cheng, *Adv. Funct. Mater.* **20** (20), 3595 (2010).
- [15] Q. H. Tian, X. Wang, G. Y. Huang and X. Y. Guo, *Nanoscale Res. Lett.* **12** (1), 214 (2017).
- [16] G. Rajeshkhanna, E. Umeshbabu, P. Justin and G. Ranga Rao, *Int. J. Hydrogen Energy* **40** (36), 12303 (2015).
- [17] Y. Jiang, C. Tang, H. Zhang, T. Shen, C. Zhang and S. Liu, *J. Mater. Chem. A*, **5**(12), 5781 (2017).
- [18] N. Zhang, Y. H. Ding, J. Y. Zhang, B. Fu, X. L. Zhang, X. F. Zheng and Y. Z. Fang, *J. Alloys Compd.* **694**, 1302 (2017).
- [19] J. Huang, T. Lei, X. Wei, X. Liu, T. Liu, D. Cao, J. Yin and G. Wang, *J. Power Sources* **232** (232), 370 (2013).
- [20] I. Rozenblit, S. Murugupillai, M. A. McArthur, M. Brochu and S. Omanovic, *Mater. Chem. Phys.* **193**, 73 (2017).
- [21] H. M. Wei, J. X. Wang, L. Yu, Y. Y. Zhang, D. W. Hou and T. F. Li, *Mater. Lett.* **187**, 11 (2017).
- [22] G. Zhu, J. Chen, Z. Zhang, Q. Kang, X. Feng, Y. Li, Z. Huang, L. Wang and Y. Ma, *Chem. Commun.* **52** (13), 2721 (2016).
- [23] W. F. Wei, X. W. Cui, W. X. Chen and D. G. Ivey, *Chem. Soc. Rev.* **40** (3), 1697 (2011).
- [24] L. Y. Lin, S. Tang, S. Q. Zhao, X. H. Peng and N. Hu, *Electrochim. Acta*, **228**, 175 (2017).
- [25] Y. X. Wen, T. F. Qin, Z. L. Wang, X. Y. Jiang, S. L. Peng, J. C. Zhang, J. Hou, F. Huang, D. Y. He and G. Z. Cao, *J. Alloys Compd.* **699**, 126 (2017).
- [26] X. Zhang, X. Meng, S. Gong, P. Li, L. e. Jin and Q. Cao, *Mater. Letter.* **179**, 73 (2016).
- [27] C. Wang, F. Li, Y. Wang, H. Qu, X. Yi, Y. Lu, Y. Qiu, Z. Zou, B. Yu and Y. Luo, *J. Alloys Compd.* **634**, 12 (2015).
- [28] K. Zhou, W. Zhou, L. Yang, J. Lu, S. Cheng, W. Mai, Z. Tang, L. Li and S. Chen, *Adv. Funct. Mater.* **25** (48), 7530 (2015).
- [29] R. N. Reddy and R. G. Reddy, *J. Power Sources*, **124** (1), 330 (2003).
- [30] P. H. Yang, Y. Ding, Z. Y. Lin, Z. W. Chen, Y. Z. Li, P. F. Qiang, M. Ebrahimi, W. J. Mai, C. P. Wong and Z. L. Wang, *Nano letter.* **14** (2), 731 (2014).
- [31] J. Yang, C. Yu, X. Fan, C. Zhao and J. Qiu, *Adv. Funct. Mater.* **25** (14), 2109 (2015).
- [32] V. Khomenko, E. Raymundo-Piñero and F. Béguin, *J. Power Sources*, **153** (1), 183 (2006).